Article

# Functional and Modeling Studies of the Transmembrane Region of the TRPM8 Channel

Gabriel Bidaux,[1,2,3] Miriam Sgobba,[4] Loic Lemonnier,[1,2] Anne-Sophie Borowiec,[1,2] Lucile Noyer,[1,2] Srdan Jovanovic,[6] Alexander V. Zholos,[5,*] and Shozeb Haider[6,*]

[1]Inserm, U1003, Laboratoire de Physiologie Cellulaire, Equipe labellisée par la Ligue contre le Cancer, Villeneuve d'Ascq, France; [2]Laboratory of Excellence, Ion Channels Science and Therapeutics, Université de Lille 1, Villeneuve d'Ascq, France; [3]Laboratoire Biophotonique Cellulaire Fonctionnelle. Institut de Recherche Interdisciplinaire, Villeneuve d'Ascq, France; [4]Centre for Cancer Research and Cell Biology, Queen's University of Belfast, Belfast, United Kingdom; [5]Department of Biophysics, Educational and Scientific Centre, "Institute of Biology" Taras Shevchenko, Kiev National University, Kiev, Ukraine; and [6]UCL School of Pharmacy, London, United Kingdom

ABSTRACT Members of the transient receptor potential (TRP) ion channel family act as polymodal cellular sensors, which aid in regulating $Ca^{2+}$ homeostasis. Within the TRP family, TRPM8 is the cold receptor that forms a nonselective homotetrameric cation channel. In the absence of TRPM8 crystal structure, little is known about the relationship between structure and function. Inferences of TRPM8 structure have come from mutagenesis experiments coupled to electrophysiology, mainly regarding the fourth transmembrane helix (S4), which constitutes a moderate voltage-sensing domain, and about cold sensor and phosphatidylinositol 4,5-bisphosphate binding sites, which are both located in the C-terminus of TRPM8. In this study, we use a combination of molecular modeling and experimental techniques to examine the structure of the TRPM8 transmembrane and pore helix region including the conducting conformation of the selectivity filter. The model is consistent with a large amount of functional data and was further tested by mutagenesis. We present structural insight into the role of residues involved in intra- and intersubunit interactions and their link with the channel activity, sensitivity to icilin, menthol and cold, and impact on channel oligomerization.

## INTRODUCTION

The transient receptor potential (TRP) ion channel family is ubiquitously present throughout mammals (1). There are 28 members of the mammalian TRP channel superfamily, which form six subfamilies based on sequence similarity and homology (2). Many TRP channels act as polymodal cellular sensors that respond to chemical and physical changes in both a local and global environment. They respond to a variety of different gating stimuli including intracellular (IC) and extracellular (EC) messengers, chemical, mechanical and osmotic stress, temperature, growth factors, and depletion of IC $Ca^{2+}$ stores (3). Activation of these nonselective cation channels triggers not only $Na^{+}$ influx and membrane depolarization, but also $Ca^{2+}$ influx from EC matrix to cytosol as well as from the endoplasmic reticulum (ER) stores to cytosol for channels located in the ER membranes (4). TRP-mediated $Ca^{2+}$ signaling leads to specific biological effects such as induction of proliferation, modulation of the electrical activity of excitable cells in the brain and heart, sensory perception, and vascular contractility. Given the importance of $Ca^{2+}$ signaling in all cell types and the role of TRP channels in regulating $Ca^{2+}$ homeostasis, it is not surprising that an abnormality in TRP channel function often results in pathogenesis of several diseases including channelopathies like mucolipidosis, polycystic kidney diseases, hypertension, and hypomagnesaemia with hypocalcaemia (2).

Among the TRP family, TRPM8 is the primary cold receptor expressed in dorsal root ganglia neurons (5,6), and is also sensitive to substances, which mimic cold sensation, such as menthol and icilin. Interestingly, TRPM8 was originally cloned from human prostate, as it is overexpressed in prostate and other tumors (7). It was found to be located at both plasma and ER membranes of prostate cells (8,9). Although endogenous TRPM8 activation is still poorly understood in human prostate, phosphatidylinositol 4,5-bisphosphate, $PIP_2$ (10), and lysophospholipids (11) regulate its activity. Furthermore, it has been reported that lysophospholipids sensitize TRPM8 to cold (12), modifying its threshold of activation that has been reported to be around 32°C in recombinant TRPM8 channels expressed in lipid bilayers (13). Taken together, studies that have characterized TRPM8 gating by menthol, icilin, and cold, concluded that conformational shifts leading to TRPM8 opening was different and dependent of the activator (14,15).

In the absence of a crystal structure, information about TRPM8 structure has been obtained mainly by site-directed mutagenesis followed by electrophysiological characterization, with the aim to define selectivity-related sites, $PIP_2$ binding sites, and both menthol and icilin binding sites

*Submitted April 27, 2015, and accepted for publication September 28, 2015.*

*Correspondence: a.zholos@althenia.org or shozeb.haider@ucl.ac.uk

Gabriel Bidaux and Miriam Sgobba contributed equally to this work.

Editor: Randall Rasmusson.



0006-3495/15/11/1840/12

http://dx.doi.org/10.1016/j.bpj.2015.09.027

(16,17). Although several critical amino acids have been identified, no binding sites have yet been clearly defined (18). TRPM8 monomers associate as homotetramers to form a nonselective cation channel whose permeability to $Ca^{2+}$ is ~0.97–3.2 compared to that for $Na^{+}$ (5,6), though selectivity filter has not been studied. Similar to all other TRPs, a functional channel is formed by four subunits where each subunit consists of six transmembrane (TM) spanning regions (S1–S6), a short pore loop between S5 and S6 and IC N- and C-terminal domains. Little is known about the TRPM8 structure-function relationship apart from that the fourth TM helix (S4) constitutes a moderate voltage-sensing domain and that both cold sensor and $PIP_2$ binding sites are located in the C-terminus of TRPM8 (19). Stabilization of the tetramers has been poorly characterized and three studies report paradoxical data. Phelps et al. (2007) suggested that TM were sufficient for tetramerization (20), whereas other teams reported that the C-terminal coiled-coil domain was sufficient by itself (21) or in addition to other domains (22). Rationalization to structure has previously been based on the low homology with voltage-gated $K^{+}$ ($K_V$) and cyclic nucleotide-gated channels (23).

In this study, we have used a combination of computational molecular modeling and experimental methodologies to examine the structure of the TRPM8 TM and pore loop regions based on their homology with the recently published structure of TRPV1 (24,25). We present structural insight into the role of residues involved in intra- and intersubunit interactions and their link with the channel activity, sensitivity to icilin, menthol, and cold, and impact on channel oligomerization.

## MATERIALS AND METHODS

### Site-directed mutagenesis

TRPM8 mutants have been performed on TRPM8 pcDNA4.TO.A vector (4) using the Phusion Site-Directed Mutagenesis Kit (Finnzymes, Waltham, MA) as recommended. Briefly, wild-type (WT) TRPM8pcDNA4 vector was amplified with polymerase chain reaction (PCR) using 5′-phosphorylated, degenerated forward primer and 5′-phosphorylated reverse primer on the adjacent sequence. Parental vectors were digested with Dpn I restrictase for 2–4 h at 37°C. After sybr green agarose gel purification with Wizard SV Gel and PCR Clean-Up System (Promega, Mannheim, Germany), linearized TRPM8mut/pcDNA4.TO.A were ligated with T4 ligase (Promega) at 14°C overnight. After transformation into JM109 bacteria, colonies were screened by PCR and plasmids were extracted before sequencing.

### Cell culture and transient transfection

Human embryonic kidney (HEK) 293 cells were grown in Dulbecco's modified Eagle's medium (Invitrogen, Glasgow, UK) supplemented with 10% fetal calf serum (Seromed, Poly-Labo, Strasbourg, France).

Cells were transfected with 2 $\mu$g of each construct and 0.2 $\mu$g of pmaxGFP using either Nucleofector (Amaxa, Gaithersburg, MD) or FuGENE HD reagent (Roche Diagnostics, Meylan, France). For control experiments, WT TRPM8 plasmid was used. Cells were used for patch-clamp experiments 24 h after transfection.

### Electrophysiology

Macroscopic membrane ion currents were recorded at 37°C using the patch-clamp technique in its whole cell configuration. The currents were acquired using a HEKA PC-9 amplifier (HEKA Elektronik Dr. Schulze GmbH, Lambrecht, Germany) and analyzed offline using Origin 6.1 software (OriginLab, Northampton, MA). Regular EC solution (osmolarity 310 mosmol/l) contained (in mM): 150 NaCl, 5 KCl, 10 HEPES, 10 Glucose, 1 $MgCl_2$, 2 $CaCl_2$, pH, 7.3 (adjusted with NaOH). Selectivity experiments were carried out at room temperature using a different EC solution of the following composition (in mM): 100 TEA-Cl, 10 HEPES, 10 glucose, pH 7.3 (adjusted with TEA-OH), in which were added 50 mM of NaCl, KCl, CsCl, or $CaCl_2$. The IC pipette solution (osmolarity 290 mosmol/l) contained (in mM): 140 CsCl, 10 HEPES, 8 EGTA, 1 $MgCl_2$, and 4 $CaCl_2$ (100 nM free $Ca^{2+}$), pH 7.3 (adjusted with CsOH). Patch pipettes were fabricated from borosilicate glass capillaries (WPI, Hitchin, UK). The resistance of the pipettes varied between 3 and 5 MΩ. Necessary supplements were added directly to the respective solutions, in concentrations that would not significantly change the osmolarity. Changes in the external solutions were carried out using a multibarrel puffing micropipette with common outflow that was positioned in close proximity to the cell under investigation. During the experiment, the cell was continuously superfused with the solution via a puffing pipette to reduce possible artifacts related to the switch from static to moving solution and vice versa.

Results are expressed as mean ± SE. Icilin was purchased from Tocris Cookson (Bristol, UK), all other chemicals were from Sigma-Aldrich (Lyon, France).

### Cell surface biotinylation

HEK293 cells were transfected with 6 $\mu$g of WT or mutant TRPM8 plasmids for 3 million cells in 10 cm dishes. After a 40h-transfection, the biotinylation assay was performed before cell homogenization in 1 ml lysis buffer. Briefly, cells were washed two times with phosphate buffer saline (PBS) complemented with 1 mM $MgCl_2$ and 0.5 mM $CaCl_2$ at pH 8.2 (PBSB). Cells were incubated in PBSB containing 0.5 mg/ml EZ-Link Sulfo-NHS-LC-LC-Biotin (Thermo Scientific (Waltham, MA) and Pierce Protein Biology Products (Waltham, MA)), on ice for 30 min. After 2 washouts with PBSB containing 1 mM Glycine, followed with 1 wash with PBS, cells were lysed in 1X RIPA buffer as described elsewhere (4). Protein concentrations were determined with BCA assay (Thermo Scientific and Pierce Protein Biology Products). 50 $\mu$g of total protein extract were frozen to be used as an internal control, because 500 $\mu$g of proteins were pulled down with 100 $\mu$l of NeutrAvidin Agarose (Thermo Scientific and Pierce Protein Biology Products) on a rotating wheel at 4°C overnight. Beads were centrifuged for 2 min at 250 × $g$ and supernatant was removed. Beads were then suspended in 1 mL of 0.5X RIPA buffer before a further centrifugation. This step was repeated two times. Finally, pelleted beads were suspended in 2X Laemmli sample buffer, and incubated at 30°C for 45 min. Samples were thereby analyzed by immunoblotting.

### Immunoblotting

Total protein and acrylamide electrophoresis were performed as described previously (26). Immunoblotting was processed as follows: after the PVDF membrane were blocked in 5% TNT-milk (15 mM Tris buffer pH 8, 140 mM NaCl, 0.05% Tween 20, and 5% nonfat dry milk) with 5% donkey serum (Chemicon International, Temecula, CA) at room temperature for 30 min, they were soaked in 1% TNT milk with either 1/1,000 anti-TRPM8 antibody (Abcam, ab109308, lot GR47573-2, 2013) or with 1/1,500 Mouse Anti-c-Myc Monoclonal Antibody (Life Technologies, Waltham, MA) at +4°C overnight. After three washes, the membranes were incubated in antirabbit IgG or antimouse IgG secondary antibodies coupled to horseradish peroxidase-linked (Chemicon

International), diluted in 3% TNT-milk (1/20,000) for 1 h before being rinsed three times. Afterward, the membranes were processed for chemiluminescent detection using Luminata Forte, Western HRP Substrate (Merck Millipore, Darmstadt, Germany) according to the manufacturer's instructions. The blots were then exposed to X-Omat AR films (Eastman Kodak, Rochester, NY).

## Computational modeling

### *Homology model of the TM region of TRPM8 and refinement of the selectivity filter*

The sequence of human TRPM8 was taken from Uniprot (Q7Z2W7). To investigate the relationship between the selectivity filter, P-helix, and SF-S6 EC loop, three homology models of the TRPM8 TM region were generated using TRPV1 structure as a template and represented three conformations of TRPV1 in open (Protein Data Bank (PDB) code 3J5Q), intermediate (PDB code 3J5R), and closed state (PDB code 3J5P). All models were generated with Modeler v9.14 (27). Sequence alignment was performed using ClustalW (28), and then manually modified to be consistent with the UNIPROT topology assignment and previous work by Kalia and Swartz (29). To enforce the homotetrameric folding of the channel, symmetry restraints were applied to backbone atoms in the four subunits. The models were subjected to conjugate gradient energy minimizations using GROMACS software (30). The quality and the stereochemical properties of the final models were assessed after each step using PROCHECK version 3.4.4 (31). Pore dimension were evaluated by the HOLE program (32). The structural figures have been made using the ICM software (33) and PyMOL (34).

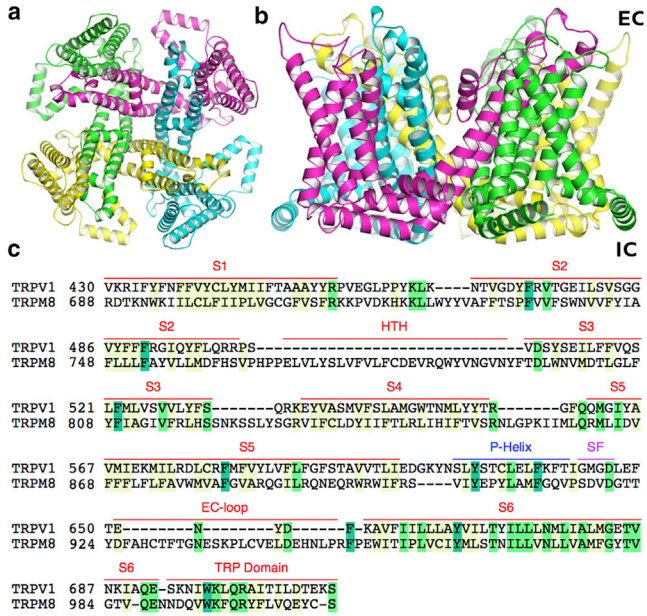


FIGURE 1 (*a*) Homology model of the human TRPM8 TM region, as viewed from the EC side. Each monomer is colored distinctly. (*b*) Side view of the human TRPM8 TM region. The IC and EC sides have been labeled. (*c*) Sequence alignment between the TM regions of human TRPV1 and TRPM8. The regions are labeled above the sequence including the predicted Helix-turn-helix segment (between S2 and S3 helices) and the EC-loop between SF and S6 helix. The colors are based on sequence conservation, where dark green represents total conservation and yellow is partial conservation. The EC and IC sides have been labeled accordingly. To see this figure in color, go online.

## RESULTS

### Structural architecture of TRPM8

TRPM8 is a homotetramer. UNIPROT topology assignment predicts cytoplasmic N- and C-terminal domains and a TM region. Each TRPM8 TM segment consists of six helices (S1–S6), a short pore helix (P-helix), and an ascending loop (between P-helix and S6), which includes the selectivity filter (SF) and an EC linker. Four SF loops, one from each subunit, along with S5-P-S6 helices, arrange around the central axis, with fourfold symmetry, to form the pore that allows the permeation of cations across the membrane (Fig. 1). Helices S1–S4 surround the central ion channel and associate with the S5-P-S6 region of the adjacent subunit, through domain swap organization (24,25). Following S6 helix is the 18–20 amino-acid $\alpha$-helical TRP domain containing the conserved WxxQ signature sequence. The TRP domain has been proposed to engage in subunit assembly or allosteric modulation of channel gating (1,23,35). This helix, which sits at the interface of the inner membrane, also interacts with the S1 and S4–S5 linker. Another short helix-turn-helix region has been predicted between S2 and S3 helices, which is similar to the TRP domain, and runs parallel along the inner leaflet of the membrane (see Fig S3 in the Supporting Material).

Three homology models of the TRPM8 TM region were built using the recently solved structures of TRPV1 as templates, in open (PDB code 3JPQ), intermediate (PDB code 3J5R), and closed (PDB code 3J5P) states. The different states are categorized based on the conformation of the residues in the SF and lower gate in the S6 helix (25). In the closed state, the ion-conducting pathway is constricted at the SF and lower gate. In the intermediate state, the SF is constricted, while the lower gate is open. Finally, in the open state, both the SF and the lower gate are expanded and the pore is dilated without any constrictions (Fig. 2). The narrowest points in the pore are observed between diagonally opposite carbonyl oxygen at $S^{917}$ in the SF and between the side chains of $V^{976}$ in the lower gate. It is worth noting that the channel pore in open conformation of TRPV1 and our model is too narrow to accommodate large cations (24,25). Nevertheless, the conformational flexibility that is observed at both, SF and lower gate, may allow TRPV1 and other TRPs like TRPM8, to assume a pore-dilated open state (24,25). This has been confirmed in a recent study, where permeation and dynamics of an open-activated TRPV1 channel was analyzed (36). The C$\alpha$ RMSD (root mean-squared deviation) between the closed (Fig. 2 *a*), intermediate (Fig. 2 *b*), and the open (Fig. 2 *c*) conformations of the models ranged between 0.8 Å and 1.5 Å. The relatively low difference in RMSD between different conformations is a result of the static nature of S1–S4 domains during channel activation within the TRP family (25). The predominant

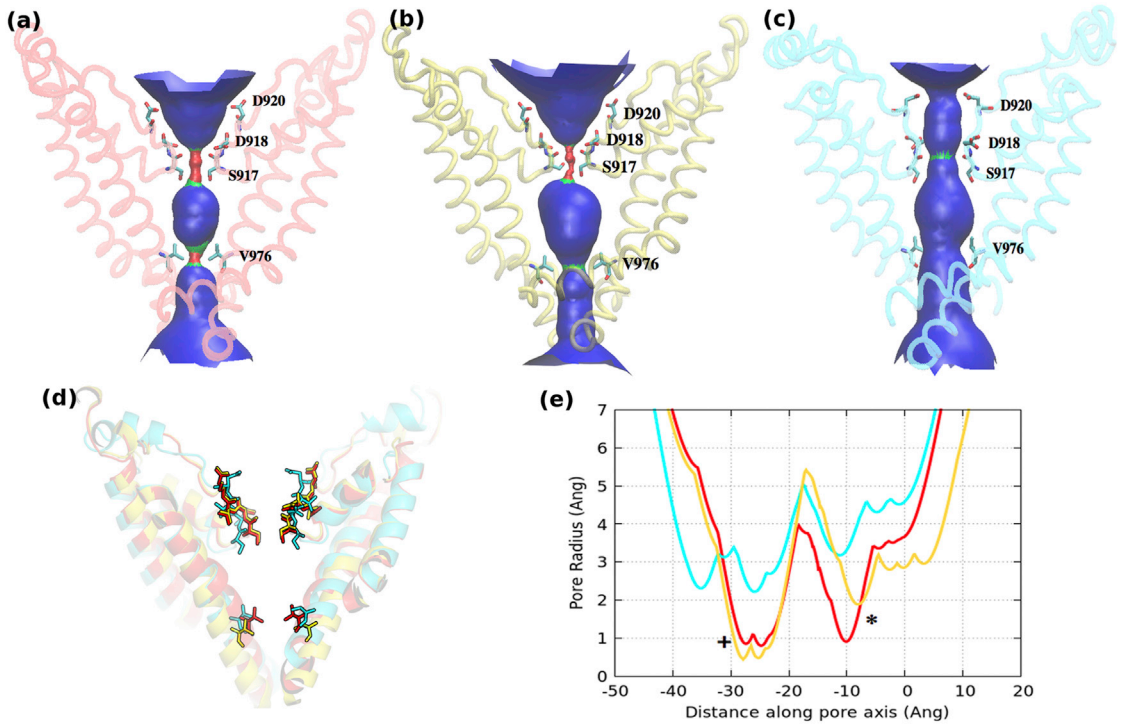


FIGURE 2 Pore profile of the human TRPM8 model in (*a*) closed/red (*b*) intermediate/yellow and (*c*) open/cyan conformations. Only two diagonally opposite subunits have been shown for clarity. The solvent accessible pathway as generated by the HOLE software is illustrated as red (radius < size of a water molecule), green (radius ~size of a water molecule), and blue (radius > size of a water molecule) surface. The residues that align the SF and the lower gate have been rendered as sticks. (*d*) Superimposition of the three models highlights the conformational changes in the SF and the lower gate. (*e*) The pore radius profile of the three models. + corresponds to the SF and * denotes the lower gate region. To see this figure in color, go online.

differences are observed only in S5-P-S6 helices. Similar to the TRPV1 structure, the pore profiles support a dual gating mechanism involving substantial conformational changes in both SF and the lower gate (24,25).

The percentage identity in the TM helices ranges between 20% and 30%. The C$\alpha$ RMSD between the model and the template is 0.9Å (closed/intermediate) and 1.2 Å (open) and lies within the expected range for proteins sharing 20–30% sequence identity (37). However, in cases where sequence identity between the template (TRPV1) and the target (TRPM8) is low, it is essential to validate the predictive power of the model by making novel mutations (38). Rationalized mutations, followed by experiments provide a structural explanation to function and confirm the robustness of the models (38–42). Despite the low sequence identity within the TRP family, all members exhibit the same conserved gating mechanism (43). The SF sequence is $^{917}$SDVD$^{920}$, where both backbone carbonyl and side-chain carboxylic oxygen atoms point into the central ion conduction pathway. The structural difference between the voltage-gated $Na^+/K^+$ and $Ca^{2+}$ channel SFs is functionally relevant for the ion permeation and selectivity. Although in $Na^+$ and $K^+$ channels, sodium and potassium ions are coordinated by the peptide backbone, in $Ca^{2+}$ channels the side chains of conserved D/E residues located in the SF are responsible for the chelation of ions (44). Atomistic structures of the SF in $Ca^{2+}$ channels have been previously modeled and different $Ca^{2+}$-coordination patterns were described, all having a ring formed by the side chains of the D/E residues located in the SF (45). TRPM8 $D^{920}$ is a highly conserved amino acid within the TRP family (Figs. 1 *C* and S1), whereas $D^{918}$ is substituted by a glutamate residue in several TRPM channels (Fig S1). Neutralization of the $D^{920}$ orthologous residue of the TRPM4 channel by an alanine substitution results in a nonfunctional channel (46), suggesting that it forms the main component of TRPM4 SF. Furthermore, mutation of the equivalent residue in TRPV1 ($D^{646}$) has also shown to result in lower sensitivity and reduced permeability to divalent cations (47–49).

In TRPM8, the $D^{918}$ and $D^{920}$ side chains from each subunit form two rings (referred to as DDDD rings), one at the top (toward the EC side of the channel) and one at the bottom of the SF. The negative charges of $D^{918}$ or $D^{920}$ have been implicated in coordinating $Ca^{2+}$ ions in the SF. The side-chain conformations adopted by $D^{918}$ and $D^{920}$ are distinct in open and closed states (Fig. 3). In the closed conformation, the negatively charged side chains of $D^{918}$ are positioned perpendicular to the pore axis and makes hydrogen bonds with the backbone nitrogen atoms of $V^{919}$ (Fig. 3, *a* and *b*). This interaction reduces the flexibility of the selectivity filter and locks it in a conformation that constricts the dimensions of the pore. In the open state, the aspartate side chains of $D^{918}$

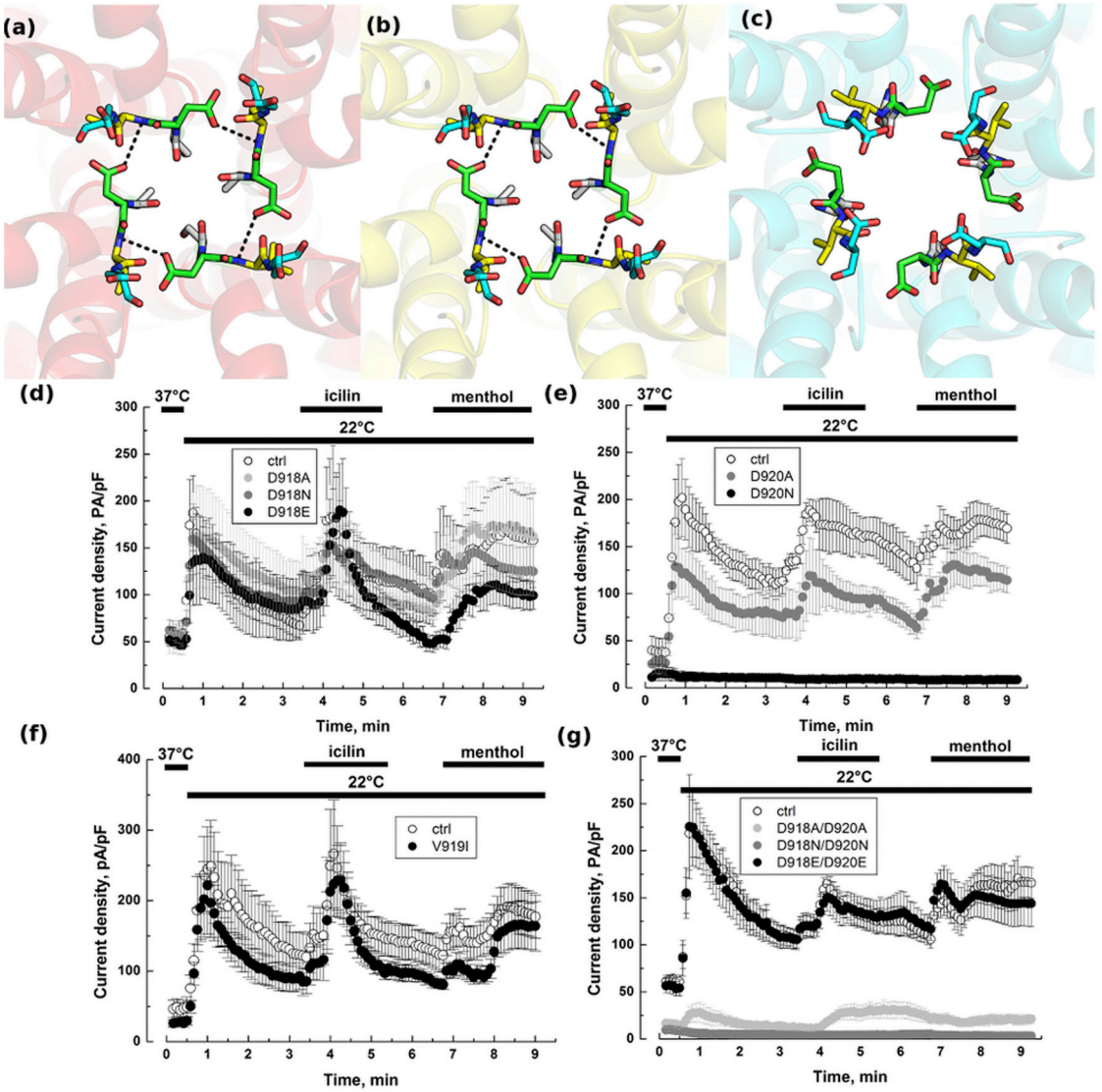


FIGURE 3 Role of DDDD rings in the selectivity filter. In the (*a*) closed/red and (*b*) intermediate/yellow conformation, $D^{918}$ makes hydrogen bonds with the backbone nitrogen of $V^{919}$. This interaction is lost in the (*c*) open/cyan state, where the side chains of $D^{918}$ are pointing into a cavity between the SF and the P-helix. The side chains of $D^{920}$ point toward the pore. Side chains of $S^{917}$ (*white*), $D^{918}$ (*green*), $V^{919}$ (*yellow*), and $D^{920}$ (*cyan*) are rendered as sticks. Whole-cell recordings at +100 mV showing TRPM8 currents induced with either cold (22°C), or icilin (10 $\mu$M), or menthol (500 $\mu$M) for HEK cells transfected with (*d*) $D^{918}$* TRPM8 mutants (*e*) $D^{920}$* TRPM8 mutants (*f*) $V^{919}$I mutant and (*g*) $D^{918}$*/$D^{920}$* double TRPM8 mutants; *represents the substituted amino acids. Cells transfected with WT TRPM8 were used as control (*ctrl*). To see this figure in color, go online.

point away from the central pore and position in a small cavity created by the rearrangement of the pore helices and the SF (Fig. 3 *c*). As a result of the tilt of the pore helix away from the central axis of the channel and conformational changes in the SF, the side chains of $D^{920}$ reorient and point toward the inner cavity of the central pore of the channel ready to coordinate $Ca^{2+}$ ion.

## Organization and function of DDDD rings in TRPM8 selectivity filter

We next investigated which and how the DDDD rings could be involved in ion conduction. We created several TRPM8 mutants before comparing their electrophysiological properties with the WT TRPM8 channel by means of the Patch-clamp technique using the whole cell configuration. As shown in Fig. 3 *d*, substitution of $D^{918}$ by alanine (*neutral, small side chain*), glutamic acid (*negatively charged, polar, longer side chain*), or asparagine (*neutral, polar, medium side chain*) had no significant effect on TRPM8 activity. Conversely, alanine and asparagine substitution of $D^{920}$ (Fig. 3 *e*) respectively reduced and almost abolished TRPM8 current in response to sequential treatment with cold (22°C), icilin (10 $\mu$M), and menthol (500 $\mu$M), whereas substitution with glutamic acid did not alter TRPM8 current (for peak current data, see the

Supporting Material). Because mutants of the TRPM8 channel were detected at the cell surface with biotinylation assay, suppression of TRPM8 current could not have been the result of misfolding or from issues in channel translocation (Fig S4). Moreover, as shown in Fig S5, these mutations did not affect channels core electrophysiological properties such as the current-voltage relationship, or general shape of the traces. Ion selectivity of WT TRPM8, $D^{918}A$ and $D^{920}A$ mutants was quantified on the basis of the shifts in reversal potentials caused by the replacement in the EC solution of 50 mM $Na^+$ with equimolar concentrations of $K^+$, $Cs^+$, or $Ca^{2+}$. Mutations did not affect permeation sequence, which remained $Ca^{2+}>K^+\approx Cs^+\approx Na^+$ as previously described (5). Recorded permeability values for WT TRPM8 ($n=14$), $D^{918}A$ ($n=7$), and $D^{920}A$ ($n=7$) mutants were respectively: $P_K/P_{Na} = 1.08 \pm 0.02$, $1.06 \pm 0.01$, and $1.08 \pm 0.02$; $P_{Cs}/P_{Na} = 1.04 \pm 0.01$, $1.03 \pm 0.01$, and $1.07 \pm 0.03$; $P_{Ca}/P_{Na} = 6.25 \pm 1.28$, $8.67 \pm 2.96$, and $5.05 \pm 0.49$, showing no significant difference between WT TRPM8 and mutants selectivity. To further understand whether the peptide backbone per se might be involved in TRPM8 SF, we substituted $V^{919}$ with an isoleucine. As illustrated in Fig. 3 *f*, $V^{919}I$ mutant did exhibit similar responses to cold, icilin, and menthol than WT TRPM8. Our results therefore suggest that the coordinated negative charge of the side chain of $D^{920}$ facilitates cations conductance, but is not by itself enough to explain the selection between cations associated with TRPM8 activity. To assess a putative complementary role of $DDDD^{918}$ ring in the pore backbone, we performed double point mutations on $D^{918}$ and $D^{920}$ (Fig. 3 *g*). Although, $D^{918}N/D^{920}N$ double mutant was inactive, a strong decrease of current was detected with the $D^{918}A/D^{920}A$ mutant (87.4%, 80.8%, and 87.5% decrease for cold, icilin, and menthol-activated currents, respectively), and no significant effect was observed with the $D^{918}E/D^{920}E$ mutant. Current reduction of the $D^{918}A/D^{920}A$ mutant without any apparent changes in channel electrophysiological properties (Fig S5) is likely triggered by the destabilization of the ion conduction pathway in the pore, which indicated a structural role for the two DDDD rings.

Finally, to determine if coordination by four $D^{920}$ is required for a functional channel, we expressed heteromeric TRPM8 ($D^{920}A$)/WT channels and determined the role of $D^{920}A$ mutation. To address this, WT TRPM8 vector was concomitantly transfected with either empty vector or with mutant TRPM8 ($D^{920}A$). Coexpression of WT TRPM8 and $D^{920}A$ mutant (Fig S6) triggers a similar drop in current amplitude than the one observed in Fig. 3 *e*, with the $D^{920}A$ homotetramers (59.9% of control for cold, 46.5% of control for icilin, and 45.1% of control for menthol). Values are presented in Table S1. With regards to our model, we concluded that mutation $D^{920}A$ did not impair oligomerization, but that these four residues are essential for the DDDD ring function.

In accordance with previous findings that orthologous residues of $D^{920}$ (TRPM8), in TRPM4, TRPV1, and TRPV6, were critical for ion conduction, we have experimentally confirmed that $D^{920}$ residue in TRPM8 channel participates to TRPM8 SF (46–48,50). However, we demonstrated that the TRPM8 SF is not operating through the exclusion of undesired ions, but rather through flow facilitation of desired ions.

## P-helix is critical for cold and menthol but not icilin activation of TRPM8

The structure of the TRPV1 channel has revealed that a short $\alpha$-helix (P-helix) is localized in close spatial conformation with S5 and S6 of the same monomer as well as with S6 of the adjacent monomer. $T^{633}$ in the P-helix of TRPV1 is critical for its activation by camphor (51). In addition, the $F^{640}$ residue, also present in the P-helix, is involved in opening/closure of TRPV1, TRPV2, and TRPV3 (52). $F^{640}$ substitution with leucine sensitized TRPV1 activity to lower capsaicin concentration and to lower temperatures than for WT TRPV1 (48). Finally, the P-helix is a dynamic component of the pore whose conformational shift participates in the gating of the TRPV1 channel (24,25) and may also be central to gating in other TRP family members (53). Because our TRPM8 structural model suggests that the P-helix conformation is similar to that of TRPV1, we investigated whether TRPM8 P-helix can be stabilized by interactions with adjacent TM domains and if it was involved in ligand gating.

$Y^{905}$ is a critical residue located at the start of the P-helix and makes $\pi$-stacking interactions with $Y^{908}$ from the same subunit. Its side chain is enclosed in a hydrophobic pocket that is surrounded by $V^{903}$, $I^{904}$, $Y^{908}$, $L^{909}$ (same subunit), and $W^{954}$ and $I^{957}$ (adjacent subunit) (Fig. 4 *a*). A tilt of P-helix, away from the pore during channel activation, positions $Y^{905}$ in close proximity to the adjacent subunit (Fig. 4 *b*). However, no hydrogen bonding is observed within this hydrophobic cluster. This is similar to P-helix interactions in several other TRP channels, including TRPV1, where the flexible architecture controls channel permeability to large cations (54,55). $Y^{905}$ substitution with an alanine, a tryptophan, or a phenylalanine led to very different consequences on TRPM8 activity. Although complete removal of the aromatic group in $Y^{905}A$ mutant totally prevented channel activation, removal of hydroxyl group in $Y^{905}F$ did not affect TRPM8 current (Fig. 4 *c*). The substitution of the benzyl side chain by an indole group strongly decreased TRPM8 current regardless of the stimulus. This suggests that $Y^{905}$ stabilize the conformation of the P-helix likely via $\pi$-stacking. As previously reported for all other current-generating TRPM8 mutants in this study, there were no apparent changes in $Y^{905}W$ and $Y^{905}F$ electrophysiological properties at the whole cell level (Fig S5).

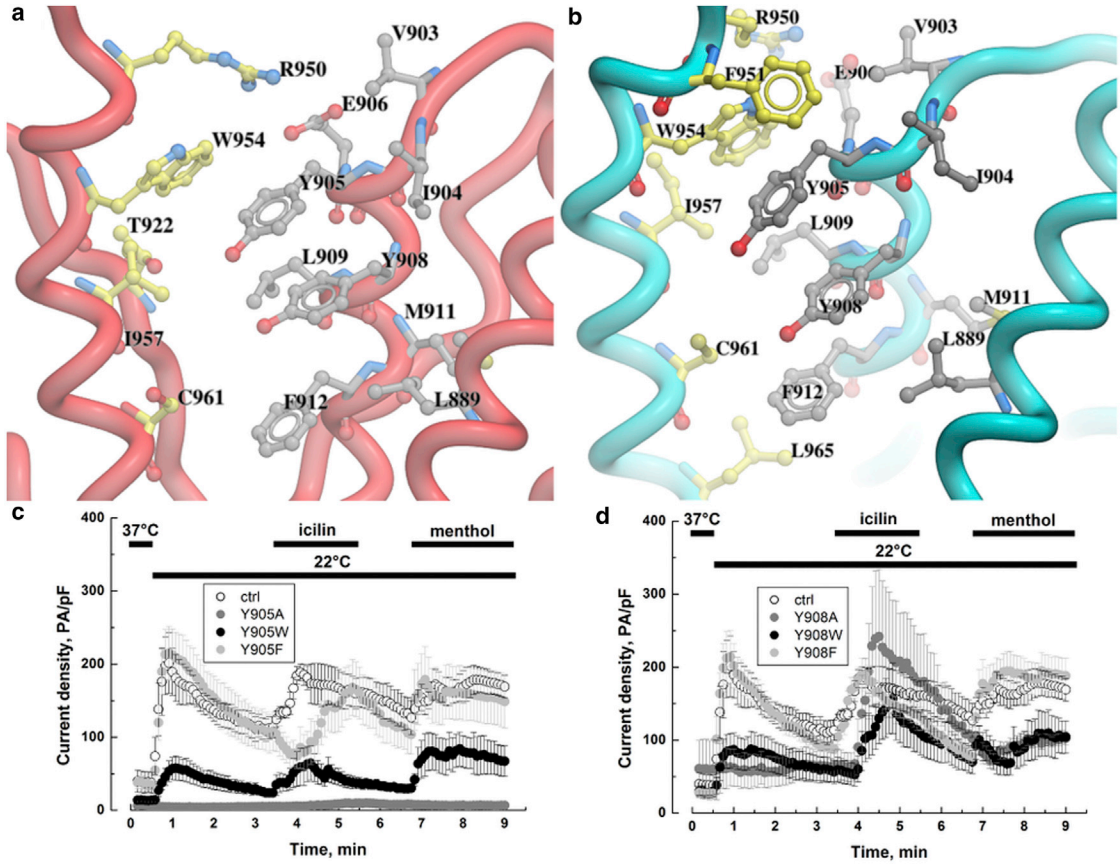


FIGURE 4 Intersubunit hydrophobic cluster between P- and S6 helices in (*a*) closed and (*b*) open conformations. The side chains from one subunit are colored gray and those from an adjacent subunit are rendered as yellow sticks. Whole-cell recordings at +100 mV of TRPM8 currents induced with either cold (22°C), or icilin (10 $\mu$M), or menthol (500 $\mu$M) for HEK cells transfected with (*c*) $Y^{905}A$, $Y^{905}F$, or $Y^{905}W$ TRPM8 mutants, and (*d*) $Y^{908}A$, $Y^{908}F$, or $Y^{908}W$ TRPM8 mutants. Cells transfected with WT TRPM8 were used as control (*ctrl*). To see this figure in color, go online.

Coexpression of $Y^{905}A$ mutation with WT TRPM8 (Fig S6) generates a dramatic decrease in channel activity (49.3%, 28%, and 46.4% respectively for cold, icilin, and menthol) but confirms that $Y^{905}A$ monomers oligomerized with WT.

$Y^{908}$ is a conserved residue among TRPM channels and its side chain is buried toward the S5–S6 helices (Fig. 4, *a* and *b*). It makes $\pi$-stacking interactions with $Y^{905}$. $Y^{908}$ mutations provided us with some new, to our knowledge, data on how TRPM8 senses cold and menthol stimuli. Suppression of the phenol side chain ($Y^{908}A$) or its substitution by an indole side chain ($Y^{908}W$) triggered an almost complete loss of sensitivity to both cold and menthol application, whereas responses to icilin were similar to WT TRPM8 (Fig. 4 *d*). Conversely, the removal of the hydroxyl group in $Y^{908}F$ did not modify TRPM8 currents in response to cold, icilin, and menthol. The mutants were properly targeted to the plasmalemma (Fig S4), and once again retained all the apparent electrophysiological properties of WT TRPM8 (Fig S5). Coexpression of $Y^{908}A$ mutant with WT TRPM8 (3:1 ratio) induced a significant decrease of cold-activated currents (34.7%), but not of menthol-activated ones (15%, Fig S6). We can thus conclude that the P-helix is involved in cold and menthol gating of the TRPM8 channel, whereas icilin activation does not involve the P-helix in the same manner. In addition, our results suggest that $Y^{908}$ could be implicated in a functional $\pi$-stacking interaction involved in cold and menthol activation of TRPM8. In our previous studies, we observed a similar effect on TRPM8 ligand gating when coexpressing TRPM8 with its short isoforms (56,57). Indeed, short TRPM8 isoforms interacted with the C-terminus of TRPM8, leading to an increased stability of the closed conformation of the channel. To our knowledge, in light of our new data, it is therefore likely that, while interacting with the TRPM8 channel, the short isoforms induce a shift of the P-helix conformation or position similar to the one operated in $Y^{908}A$ mutant. Finally, this study confirms that conformational shifts occurring during cold and menthol activation of TRPM8 are different from the one occurring after icilin stimulation (56). Strikingly, the two key tyrosines of the P-helix, $Y^{905}$, and $Y^{908}$, exhibited $\pi$-stacking interactions.

$E^{906}$ is another important amino acid involved in P-helix function. It forms an ion pair interaction with $R^{950}$, present

in the SF-S6 EC loop of the adjacent subunit (Fig. 5 *a*). The structural role of $E^{906}$ in maintaining the interactions to spatially position the P-helix is assessed by its crucial role in the channel. Substitution of $E^{906}$ with alanine completely inactivates the TRPM8 channel (Fig. 5 *b*), although its substitution with a polar neutral side chain of glutamine partially restores its activity (Fig. 5 *b*). As presented in Fig S6, coexpression experiments of $E^{906}A$ with WT TRPM8 (3:1 ratio) show a significant drop in cold-mediated TRPM8 current. Similarly, $R^{950}$ substitution to glutamate exhibited no detectable current when expressed in HEK cells, though 1) channel expression at the cell surface was found to remain unchanged (Fig S4) and 2) heteromultimerization of $R^{950}$ with WT TRPM8 showed a detectable current (Fig S6).

The side chain of $E^{893}$ (S5 helix) is positioned adjacent to $Y^{908}$ in the P-helix (Fig. 6). The side chains do not form bonded interactions with any neighboring residues in both open and closed states. The expression of $E^{893}A$ mutants resulted in a near loss of detectable currents. The side chains of $E^{893}$ are involved in packing interactions and a mutation to the short hydrophobic side chain of alanine is not tolerated at this position (Fig. 6).

## Stabilization of the SF-to-S6 EC loop

$N^{934}$ residue is localized in the EC loop formed between SF and S6. It has been reported to be *N*-glycosylated and to modulate cold and menthol-sensitivity of the channel (58). It is thought that $C^{929}$ and $C^{940}$ residues could form a disulfide bond (59), stabilizing the EC loop (Fig. 5 *d*). In this study, the authors also demonstrated that the loss of this disulphide bond did not challenge mutant tetramerization. We therefore studied the stabilization of this EC loop by means of its interaction with other domains of the TRPM8 pore.

First, we confirmed that substitution of $C^{940}$ with either glycine or arginine completely abolished TRPM8 activity (Fig. 5, *e* and *f*). The mutant channel was found at the cell surface, though to a lesser amount than in control (Fig S4). Coexpression experiments of WT TRPM8 with both $C^{940}$ mutants in a 1:3 ratio led to normal channel activity (Fig S6).

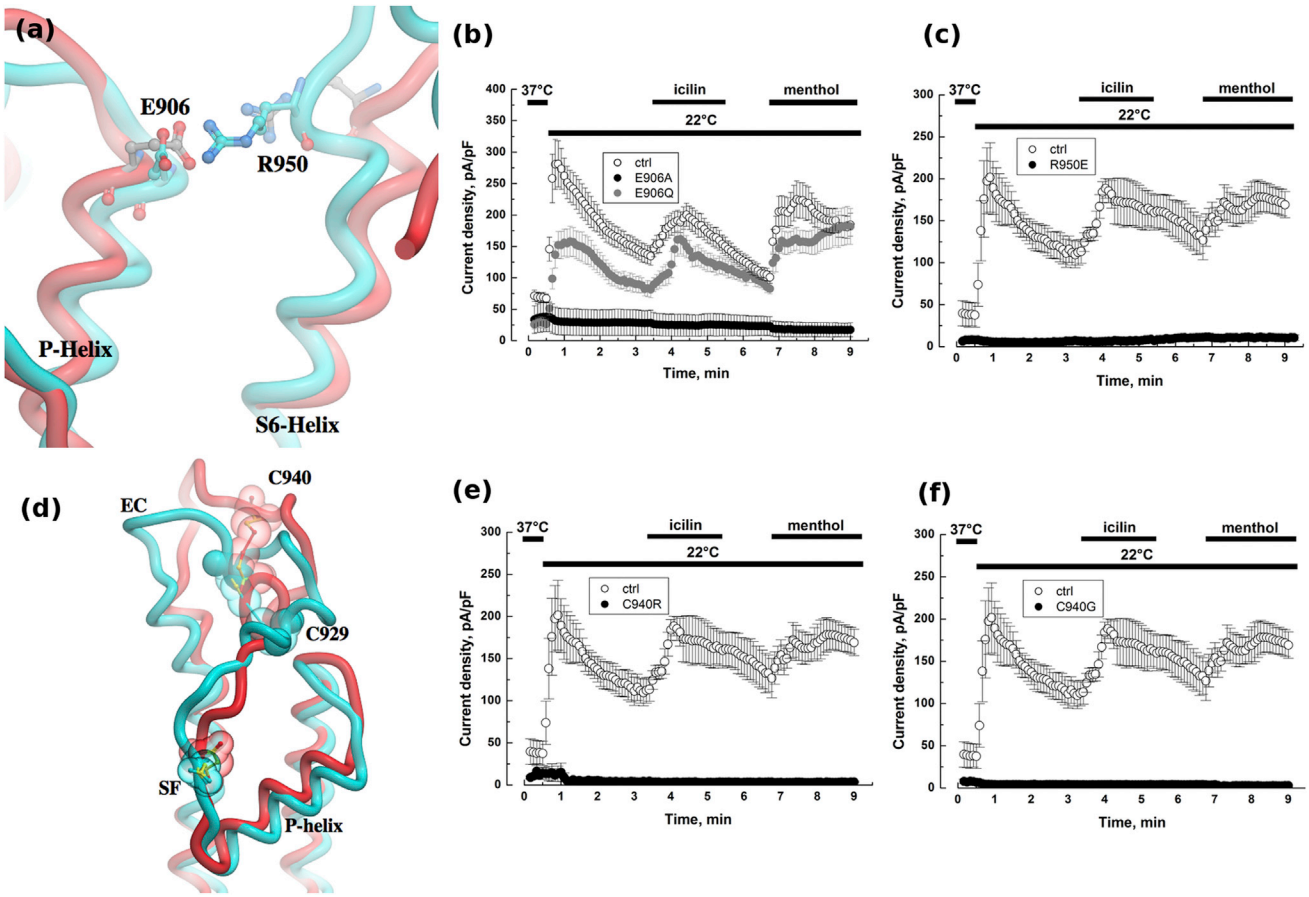


FIGURE 5 Residues involved in conformation of P-helix and of SF-to-S6 EC loop. The closed conformation is colored red and the open state in cyan. The interactions between (*a*) $E^{906}$ and $R^{950}$ are rendered as sticks and (*d*) disulphide bond formed by $C^{929}$-$C^{940}$ are illustrated as transparent balls. Whole-cell recordings at +100 mV of TRPM8 currents induced with either cold (22°C), or icilin (10 $\mu$M), or menthol (500 $\mu$M) for HEK cells transfected with (*b*) $E^{906}A$ or $E^{906}Q$ TRPM8 mutant (*c*) $R^{950}E$ TRPM8 mutant (*e*) $C^{940}R$ TRPM8 mutant and (*f*) $C^{940}G$ TRPM8 mutant. Cells transfected with WT TRPM8 were used as control (*ctrl*). To see this figure in color, go online.

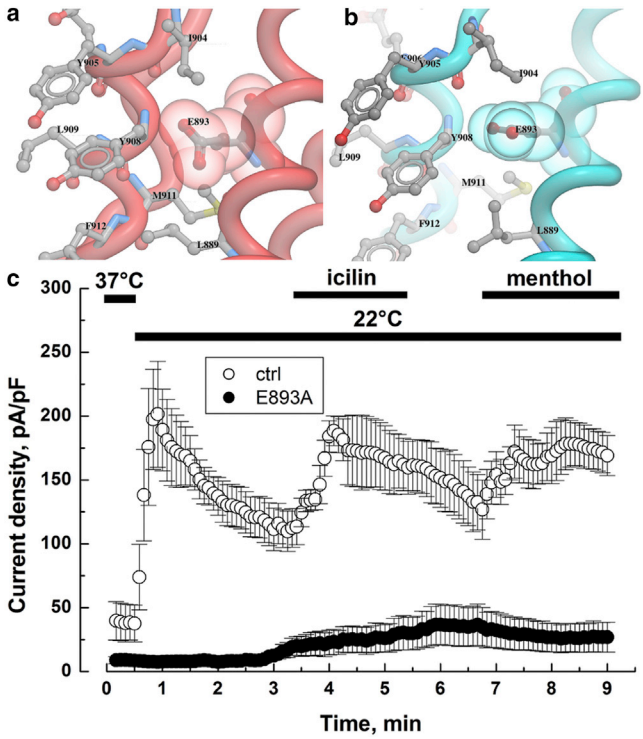


FIGURE 6 Molecular interactions of $E^{893}$ in (*a*) closed/red and (*b*) open/cyan conformation. (*c*) Whole-cell recordings at +100 mV of TRPM8 currents induced with either cold (22°C), or icilin (10 $\mu$M), or menthol (500 $\mu$M) for HEK cells transfected with $E^{893}$A TRPM8 mutant. To see this figure in color, go online.

## DISCUSSION

### Selectivity filter in TRPM8 channels

Two models of the selectivity filter are classically recognized for ion channels: the oxygen-coordinated backbone of $Na^+$ and $K^+$ channels (60) and a ring of D/E residues in the outer mouth of $Ca^{2+}$-selective channels (44). Comparatively, the great family of TRP channels can be divided into three groups characterized with their ion selectivity: 1) calcium-selective TRPV5 and TRPV6 channels (61), 2) monovalent-selective TRPM4 and TRPM5 (62), and 3) nonselective cationic channels, such as TRPM8 ($P_{Ca}/P_{Na} = 3$ (5)). Several studies and our current work have demonstrated the importance of the DDDD ring in the outer mouth of the pore in TRPV5 ($D^{542}$), TRPV6 ($D^{541}$), TRPM4 ($D^{984}$) (46,63,64), and TRPM8 ($D^{920}$) channels. Substitution of this aspartic acid with short and neutral alanine significantly decreases current density in TRPV5 and TRPV6 channels and modifies slightly the $Ca^{2+}$-selectivity. Nilius and co-workers (63) explained that the side chains of the DDDD ring were essential to stabilize the diameter of the TRPV6 outer pore at ~5.2 Å. One should note that the hydrated $Ca^{2+}$ diameter is ~4.1 Å, whereas $Na^+$ and $K^+$ diameters are 3.6 and 3.3 Å, respectively (65). Substitution of this negatively charged and polar DDDD ring with an uncharged but polar NNNN ring whose side-chains length are similar, decrease calcium permeability and slightly decrease the monovalent current density without affecting the monovalent selectivity (66). This demonstrated that the electronegative oxygen of this side chain (at physiological pH) cannot fully substitute for the negative charge of aspartate to confer $Ca^{2+}$ permeability and facilitates transportation of monovalent ions with the same efficiency. Furthermore, Nilius et al. (46) demonstrated that swapping the TRPV6 SF to TRPM4 channels makes this latter permeable to $Ca^{2+}$, even though it does not confer TRPV6 conductance. Moreover, TRPM4 SF is characterized by a second inner ring of DDDD side chains, which have been demonstrated to be involved in stabilization of the SF (46).

In this study, we have demonstrated that the open state conformation of the TRPM8 SF shows a mix pattern of TRPV5/V6 SF and TRPM4/5 SF. We have identified that the DDDD ring conserved in the TRP family was essential for the pore of TRPM8. Similar to TRPV5, we identified that both the length of the side chain and negative charges are essential in TRPM8. However, conversely to TRPV5/V6 SF (50,66), the negative charge of TRPM8 $D^{920}$ does not select divalent cations all by itself, but rather participates to the facilitation of all cation conductances. The second DDDD ring, conserved in TRPM4, is not involved in the SF function of the TRPM8 channel because its single mutation does not significantly alter TRPM8 current, contrary to what happens in TRPM4 (46). However, when the two DDDD rings were mutated to alanine, no current was recorded. This suggests that the two DDDD rings may structurally participate in the stabilization of the pore, likely by forming coordinated repulsive forces, even though only the most outward ring is necessary for coordination of cations. It is also important to note the lack of apparent effect that these mutations had on channel electrophysiological properties such as the current-voltage relationship and reversal potential. This leads us to conclude that all the mutants tested in the current study do not significantly impact TRPM8 channel selectivity for cations, as demonstrated for $D^{918}$A and $D^{920}$A.

### P-helix involvement in the activation of the TRPM8 channel

Although the structural determinants of SF activity have been studied in TRP channels, the function and role of P-helix is less described. Only two studies reported on the role of the P-helix structure in 1) Camphor sensitivity of TRPV1 (51) and 2) in pH sensitivity of TRPV5 (53). In this study, we emphasize the close interdependence between P-Helix and external loop linking SF and TM domain S6 (SF-S6 EC loop). Similar to previous work by McIntyre and co-workers (59), removal of the disulfide bond ($C^{929}$-$C^{940}$) of TRPM8 did not impair its translocation to plasmalemma in cell surface biotinylation assay. We therefore believe

that the absence of TRPM8 ($C^{940}R$) current is more related to an intrinsic issue of the channel than to a matter of translocation efficacy. Also, the SF-S6 EC loop interacts with the P-helix via the $E^{906}$-$R^{950}$ ion pair interaction. Disruption of the disulphide bond in the SF-S6 EC loop is likely to trigger a conformational change that alters interaction with the P-helix (59). We also demonstrated that $Y^{908}$ in the P-helix is crucial for menthol and cold-mediated TRPM8 activity, even though it is not involved in icilin sensitivity. By analogy with TRPV1 (51) and TRPV5 (53), we propose that either menthol binds to the P-helix or that the menthol binding site on TRPM8 (S1–S2 pocket) induces a conformational shift of the pore domain and requires rotation of the P-helix. In previous work, we demonstrated that short non-channel TRPM8 isoforms (sM8-6) (67,68) stabilizes the TRPM8 channel in its closed conformation leading to a decrease in menthol and cold sensitivity, but without modifying icilin sensitivity. We further demonstrated that this isoform could interact with the cytosolic C-terminus of TRPM8 that consequently maintains the pore in closed conformation. However, because sM8-6 isoform does not interfere with the icilin-activated current density (67), it is very unlikely that sM8-6 isoform interacts directly with the P-helix. Altogether, our results suggest, for the first time, to our knowledge, a complex physical link between the C-terminus, P-helix, and the SF-S6 EC loop required for the menthol and cold-mediated opening of the TRPM8 channel. Other studies have highlighted the requirement of S1 and S2 (18) helices, S4 voltage-sensor (69), and C-terminus (70) in menthol-mediated TRPM8 opening. In the light of current knowledge, we propose that 1) menthol induces a large shift of TRPM8 conformation involving several distinct domains, 2) cold induces conformation shift of a module composed of C-terminus, P-helix, and SF-S6 EC loop, whereas 3) icilin activation appeared to be restricted to the IC loop between S2 and S3 (71), S2 (18), and S3 TM domains (71).

## CONCLUSIONS

In conclusion, we have systematically constructed a model of the TM region of the TRPM8 channel. Our experimental results and some published data provide significant validation of the model, as none of this was used in its construction. The model was further tested based on novel, to our knowledge, mutagenesis and functional analysis. Our results led us to conclude that the ring formed by $D^{920}$ in the selectivity filter is not enough to fully account for cation conduction, but rather facilitates it, and that the P-helix and SF-S6 EC loop are involved in menthol and cold sensitivity. The model predicts several interactions in the P-helix and SF-S6 EC loop that are important in stabilization of a functional conformation of the channel. In the absence of any crystal structure, this model provides specific suggestions toward understanding the TRPM8 structure-function relationship.

## SUPPORTING MATERIAL

Six figures and one table are available at http://www.biophysj.org/biophysj/supplemental/S0006-3495(15)00998-4.

## AUTHOR CONTRIBUTIONS

G.B., L.L., A.S.B., and L.N. conducted the experiments; M.S., S.J., and S.H. constructed the molecular model, G.B., L.L., M.S., and S.H. wrote the article, G.B., A.Z., and S.H. designed the study.

## ACKNOWLEDGMENTS

S.H. is funded by the UCL Excellence Fellowship Programme.

## REFERENCES

1. Venkatachalam, K., and C. Montell. 2007. TRP channels. *Annu. Rev. Biochem.* 76:387–417.
2. Nilius, B., G. Owsianik, …, J. A. Peters. 2007. Transient receptor potential cation channels in disease. *Physiol. Rev.* 87:165–217.
3. Clapham, D. E. 2003. TRP channels as cellular sensors. *Nature.* 426:517–524.
4. Bidaux, G., M. Flourakis, …, N. Prevarskaya. 2007. Prostate cell differentiation status determines transient receptor potential melastatin member 8 channel subcellular localization and function. *J. Clin. Invest.* 117:1647–1657.
5. McKemy, D. D., W. M. Neuhausser, and D. Julius. 2002. Identification of a cold receptor reveals a general role for TRP channels in thermosensation. *Nature.* 416:52–58.
6. Peier, A. M., A. Moqrich, …, A. Patapoutian. 2002. A TRP channel that senses cold stimuli and menthol. *Cell.* 108:705–715.
7. Tsavaler, L., M. H. Shapero, …, R. Laus. 2001. Trp-p8, a novel prostate-specific gene, is up-regulated in prostate cancer and other malignancies and shares high homology with transient receptor potential calcium channel proteins. *Cancer Res.* 61:3760–3769.
8. Thebault, S., L. Lemonnier, …, N. Prevarskaya. 2005. Novel role of cold/menthol-sensitive transient receptor potential melastatine family member 8 (TRPM8) in the activation of store-operated channels in LNCaP human prostate cancer epithelial cells. *J. Biol. Chem.* 280: 39423–39435.
9. Zhang, L., and G. J. Barritt. 2004. Evidence that TRPM8 is an androgen-dependent Ca2+ channel required for the survival of prostate cancer cells. *Cancer Res.* 64:8365–8373.
10. Rohács, T., C. M. Lopes, …, D. E. Logothetis. 2005. PI(4,5)P2 regulates the activation and desensitization of TRPM8 channels through the TRP domain. *Nat. Neurosci.* 8:626–634.
11. Vanden Abeele, F., A. Zholos, …, N. Prevarskaya. 2006. Ca2+-independent phospholipase A2-dependent gating of TRPM8 by lysophospholipids. *J. Biol. Chem.* 281:40174–40182.
12. Andersson, D. A., M. Nash, and S. Bevan. 2007. Modulation of the cold-activated channel TRPM8 by lysophospholipids and polyunsaturated fatty acids. *J. Neurosci.* 27:3347–3355.
13. Zakharian, E., C. Cao, and T. Rohacs. 2010. Gating of transient receptor potential melastatin 8 (TRPM8) channels activated by cold and chemical agonists in planar lipid bilayers. *J. Neurosci.* 30:12526–12534.
14. Baez, D., N. Raddatz, …, R. Latorre. 2014. Gating of thermally activated channels. *Curr. Top. Membr.* 74:51–87.
15. Cohen, M. R., and V. Y. Moiseenkova-Bell. 2014. Structure of thermally activated TRP channels. *Curr. Top. Membr.* 74:181–211.
16. Latorre, R., S. Brauchi, …, G. Vargas. 2007. ThermoTRP channels as modular proteins with allosteric gating. *Cell Calcium.* 42:427–438.

17. Latorre, R., S. Brauchi, …, P. Orio. 2011. A cool channel in cold transduction. *Physiology (Bethesda).* 26:273–285.
18. Bandell, M., A. E. Dubin, …, A. Patapoutian. 2006. High-throughput random mutagenesis screen reveals TRPM8 residues specifically required for activation by menthol. *Nat. Neurosci.* 9:493–500.
19. Brauchi, S., G. Orta, …, R. Latorre. 2007. Dissection of the components for PIP2 activation and thermosensation in TRP channels. *Proc. Natl. Acad. Sci. USA.* 104:10246–10251.
20. Phelps, C. B., and R. Gaudet. 2007. The role of the N-terminus and transmembrane domain of TRPM8 in channel localization and tetramerization. *J. Biol. Chem.* 282:36474–36480.
21. Tsuruda, P. R., D. Julius, and D. L. Minor, Jr. 2006. Coiled coils direct assembly of a cold-activated TRP channel. *Neuron.* 51:201–212.
22. Erler, I., D. M. Al-Ansary, …, B. A. Niemeyer. 2006. Trafficking and assembly of the cold-sensitive TRPM8 channel. *J. Biol. Chem.* 281:38396–38404.
23. Latorre, R., C. Zaelzer, and S. Brauchi. 2009. Structure-functional intimacies of transient receptor potential channels. *Q. Rev. Biophys.* 42:201–246.
24. Liao, M., E. Cao, …, Y. Cheng. 2013. Structure of the TRPV1 ion channel determined by electron cryo-microscopy. *Nature.* 504:107–112.
25. Cao, E., M. Liao, …, D. Julius. 2013. TRPV1 structures in distinct conformations reveal activation mechanisms. *Nature.* 504:113–118.
26. Beck, B., G. Bidaux, …, N. Prevarskaya. 2007. Prospects for prostate cancer imaging and therapy using high-affinity TRPM8 activators. *Cell Calcium.* 41:285–294.
27. Sali, A., and T. L. Blundell. 1993. Comparative protein modelling by satisfaction of spatial restraints. *J. Mol. Biol.* 234:779–815.
28. Larkin, M. A., G. Blackshields, …, D. G. Higgins. 2007. Clustal W and Clustal X version 2.0. *Bioinformatics.* 23:2947–2948.
29. Kalia, J., and K. J. Swartz. 2013. Exploring structure-function relationships between TRP and Kv channels. *Sci. Rep.* 3:1523.
30. Pronk, S., S. Páll, …, E. Lindahl. 2013. GROMACS 4.5: a high-throughput and highly parallel open source molecular simulation toolkit. *Bioinformatics.* 29:845–854.
31. Laskowski, R. A., M. W. MacAuthor, …, J. M. Thornton. 1993. PROCHECK: a program to check the stereochemical quality of protein structures. *J. Appl. Cryst.* 26:283–291.
32. Smart, O. S., J. G. Neduvelil, …, M. S. Sansom. 1996. HOLE: a program for the analysis of the pore dimensions of ion channel structural models. *J. Mol. Graph.* 14:354–360, 376.
33. Abagyan, R., M. Totrov, and D. Kuznetsov. 1994. ICM - A new method for protein modeling and design: applications to docking and structure prediction from the distorted native conformation. *J. Comput. Chem.* 15:488–506.
34. Schrödinger, LLC. The PyMOL Molecular Graphics System.
35. Ramsey, I. S., M. Delling, and D. E. Clapham. 2006. An introduction to TRP channels. *Annu. Rev. Physiol.* 68:619–647.
36. Darré, L., S. Furini, and C. Domene. 2015. Permeation and dynamics of an open-activated TRPV1 channel. *J. Mol. Biol.* 427:537–549.
37. Russell, R. B., M. A. Saqi, …, M. J. Sternberg. 1997. Recognition of analogous and homologous protein folds: analysis of sequence and structure conservation. *J. Mol. Biol.* 269:423–439.
38. Antcliff, J. F., S. Haider, …, F. M. Ashcroft. 2005. Functional analysis of a structural model of the ATP-binding site of the KATP channel Kir6.2 subunit. *EMBO J.* 24:229–239.
39. Haider, S., A. I. Tarasov, …, F. M. Ashcroft. 2007. Identification of the PIP2-binding site on Kir6.2 by molecular modelling and functional analysis. *EMBO J.* 26:3749–3759.
40. Rapedius, M., S. Haider, …, S. J. Tucker. 2006. Structural and functional analysis of the putative pH sensor in the Kir1.1 (ROMK) potassium channel. *EMBO Rep.* 7:611–616.
41. Proks, P., C. Girard, …, F. M. Ashcroft. 2005. A gating mutation at the internal mouth of the Kir6.2 pore is associated with DEND syndrome. *EMBO Rep.* 6:470–475.
42. Trapp, S., S. Haider, …, F. M. Ashcroft. 2003. Identification of residues contributing to the ATP binding site of Kir6.2. *EMBO J.* 22:2903–2912.
43. Palovcak, E., L. Delemotte, …, V. Carnevale. 2015. Comparative sequence analysis suggests a conserved gating mechanism for TRP channels. *J. Gen. Physiol.* 146:37–50.
44. Sather, W. A., and E. W. McCleskey. 2003. Permeation and selectivity in calcium channels. *Annu. Rev. Physiol.* 65:133–159.
45. Cheng, R. C., D. B. Tikhonov, and B. S. Zhorov. 2010. Structural modeling of calcium binding in the selectivity filter of the L-type calcium channel. *Eur. Biophys. J.* 39:839–853.
46. Nilius, B., J. Prenen, …, T. Voets. 2005. The selectivity filter of the cation channel TRPM4. *J. Biol. Chem.* 280:22899–22906.
47. García-Martínez, C., C. Morenilla-Palao, …, A. Ferrer-Montiel. 2000. Identification of an aspartic residue in the P-loop of the vanilloid receptor that modulates pore properties. *J. Biol. Chem.* 275:32552–32558.
48. Winter, Z., A. Buhala, …, Z. Oláh. 2013. Functionally important amino acid residues in the transient receptor potential vanilloid 1 (TRPV1) ion channel–an overview of the current mutational data. *Mol. Pain.* 9:30.
49. Mohapatra, D. P., and C. Nau. 2003. Desensitization of capsaicin-activated currents in the vanilloid receptor TRPV1 is decreased by the cyclic AMP-dependent protein kinase pathway. *J. Biol. Chem.* 278:50080–50090.
50. Voets, T., A. Janssens, …, B. Nilius. 2004. Outer pore architecture of a Ca2+-selective TRP channel. *J. Biol. Chem.* 279:15223–15230.
51. Marsakova, L., F. Touska, …, V. Vlachova. 2012. Pore helix domain is critical to camphor sensitivity of transient receptor potential vanilloid 1 channel. *Anesthesiology.* 116:903–917.
52. Myers, B. R., C. J. Bohlen, and D. Julius. 2008. A yeast genetic screen reveals a critical role for the pore helix domain in TRP channel gating. *Neuron.* 58:362–373.
53. Yeh, B. I., Y. K. Kim, …, C. L. Huang. 2005. Conformational changes of pore helix coupled to gating of TRPV5 by protons. *EMBO J.* 24:3224–3234.
54. Chung, M. K., A. D. Güler, and M. J. Caterina. 2008. TRPV1 shows dynamic ionic selectivity during agonist stimulation. *Nat. Neurosci.* 11:555–564.
55. Salazar, H., A. Jara-Oseguera, …, T. Rosenbaum. 2009. Structural determinants of gating in the TRPV1 channel. *Nat. Struct. Mol. Biol.* 16:704–710.
56. Bidaux, G., B. Beck, …, N. Prevarskaya. 2011. Regulation of activity of transient receptor potential melastatin 8 (TRPM8) channel by its short isoforms. *J. Biol. Chem.* 287:2948–2962.
57. Fernandez, J. A., R. Skryma, …, A. V. Zholos. 2011. Short isoforms of the cold receptor TRPM8 inhibit channel gating by mimicking heat action rather than chemical inhibitors. *J. Biol. Chem.* 287:2963–2970.
58. Pertusa, M., R. Madrid, …, F. Viana. 2012. *N*-glycosylation of TRPM8 ion channels modulates temperature sensitivity of cold thermoreceptor neurons. *J. Biol. Chem.* 287:18218–18229.
59. Dragoni, I., E. Guida, and P. McIntyre. 2006. The cold and menthol receptor TRPM8 contains a functionally important double cysteine motif. *J. Biol. Chem.* 281:37353–37360.
60. Khalili-Araghi, F., E. Tajkhorshid, and K. Schulten. 2006. Dynamics of K+ ion conduction through Kv1.2. *Biophys. J.* 91:L72–L74.
61. den Dekker, E., J. G. Hoenderop, …, R. J. Bindels. 2003. The epithelial calcium channels, TRPV5 & TRPV6: from identification towards regulation. *Cell Calcium.* 33:497–507.
62. Ullrich, N. D., T. Voets, …, B. Nilius. 2005. Comparison of functional properties of the Ca2+-activated cation channels TRPM4 and TRPM5 from mice. *Cell Calcium.* 37:267–278.
63. Voets, T., A. Janssens, …, B. Nilius. 2003. Mg2+-dependent gating and strong inward rectification of the cation channel TRPV6. *J. Gen. Physiol.* 121:245–260.

64. Dodier, Y., F. Dionne, …, L. Parent. 2007. Topology of the selectivity filter of a TRPV channel: rapid accessibility of contiguous residues from the external medium. *Am. J. Physiol. Cell Physiol.* 293:C1962–C1970.

65. Conway, B. E. 1982. Ionic hydration in chemistry and biophysics. *J. Solut. Chem.* 11:221–222.

66. Nilius, B., R. Vennekens, …, R. J. Bindels. 2001. The single pore residue Asp-542 determines Ca2+ permeation and Mg2+ block of the epithelial Ca2+ channel. *J. Biol. Chem.* 276:1020–1025.

67. Bidaux, G., B. Beck, …, N. Prevarskaya. 2012. Regulation of activity of transient receptor potential melastatin 8 (TRPM8) channel by its short isoforms. *J. Biol. Chem.* 287:2948–2962.

68. Fernández, J. A., R. Skryma, …, A. V. Zholos. 2012. Short isoforms of the cold receptor TRPM8 inhibit channel gating by mimicking heat action rather than chemical inhibitors. *J. Biol. Chem.* 287:2963–2970.

69. Voets, T., G. Owsianik, …, B. Nilius. 2007. TRPM8 voltage sensor mutants reveal a mechanism for integrating thermal and chemical stimuli. *Nat. Chem. Biol.* 3:174–182.

70. Brauchi, S., G. Orta, …, R. Latorre. 2006. A hot-sensing cold receptor: C-terminal domain determines thermosensation in transient receptor potential channels. *J. Neurosci.* 26:4835–4840.

71. Chuang, H. H., W. M. Neuhausser, and D. Julius. 2004. The super-cooling agent icilin reveals a mechanism of coincidence detection by a temperature-sensitive TRP channel. *Neuron.* 43:859–869.

# Functional and Modelling Studies of the Transmembrane Region of the TRPM8 channel

Gabriel Bidaux et al.

## Supplementary Information

**Supplementary Figure S1:**

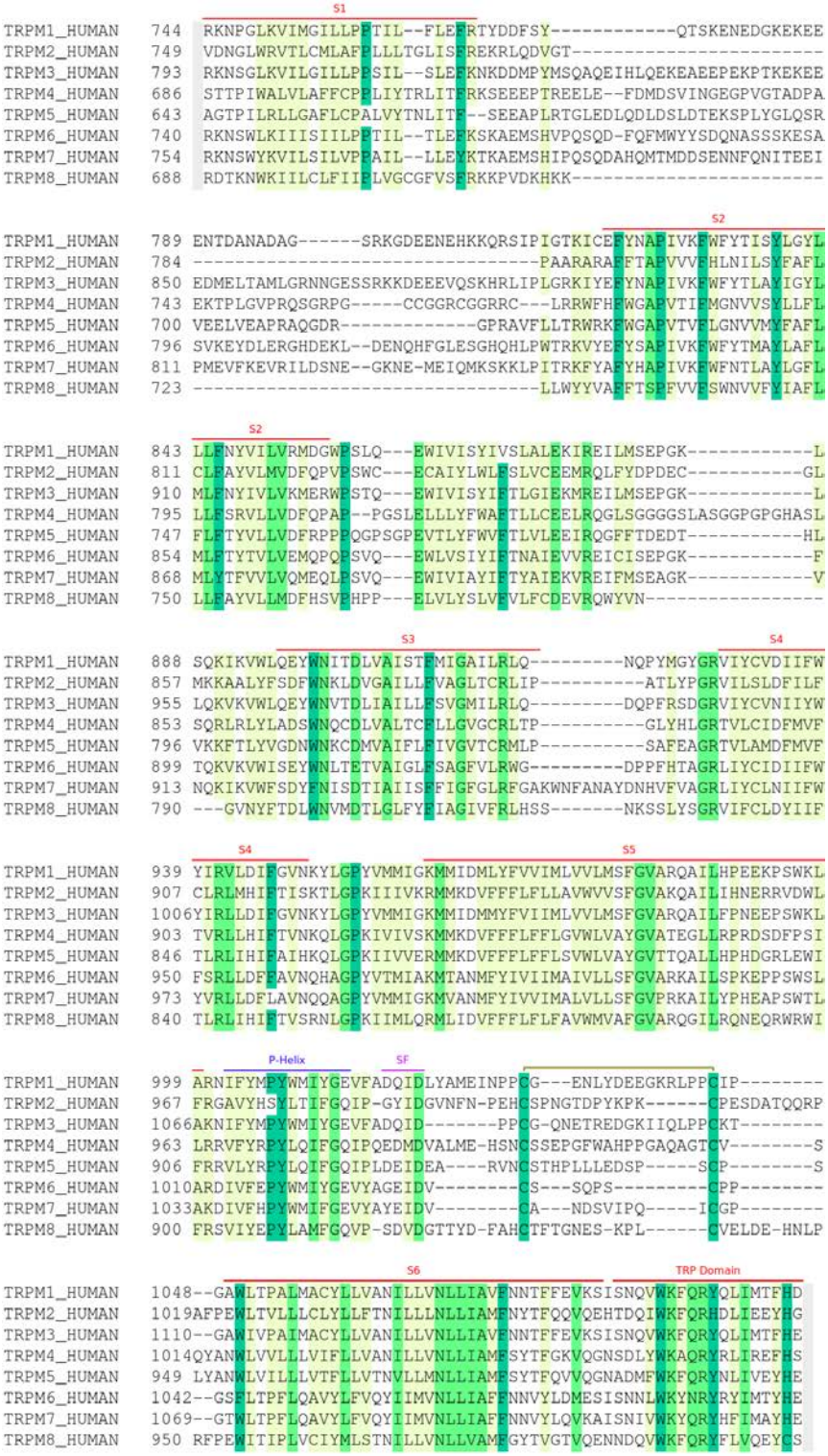


**Supplementary Figure S1.** Multiple sequence alignment of the transmembrane region within the TRPM ion channel family.

**Supplementary Figure S2:**

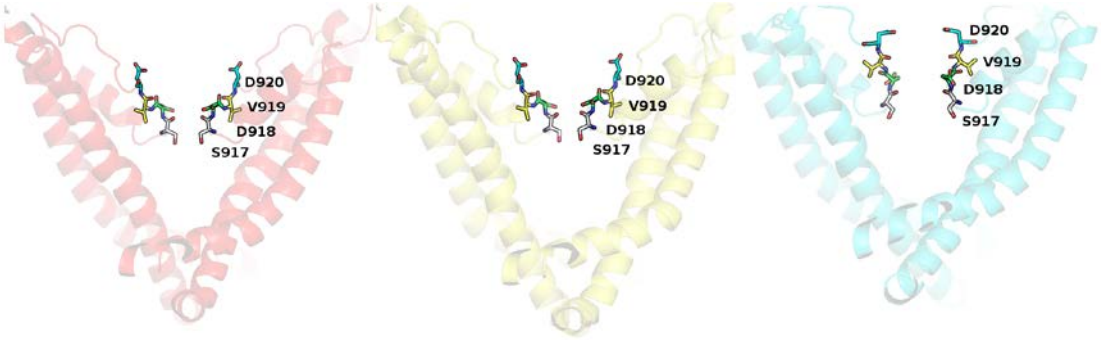


**Supplementary Figure S2.** Side view of the pore and the conformation of residues in the selectivity filter. The three conformations represent the closed (red), intermediate (yellow) and closed (cyan) states. Only two, diagonally opposite subunits have been shown for clarity.

**Supplementary Figure S3:**

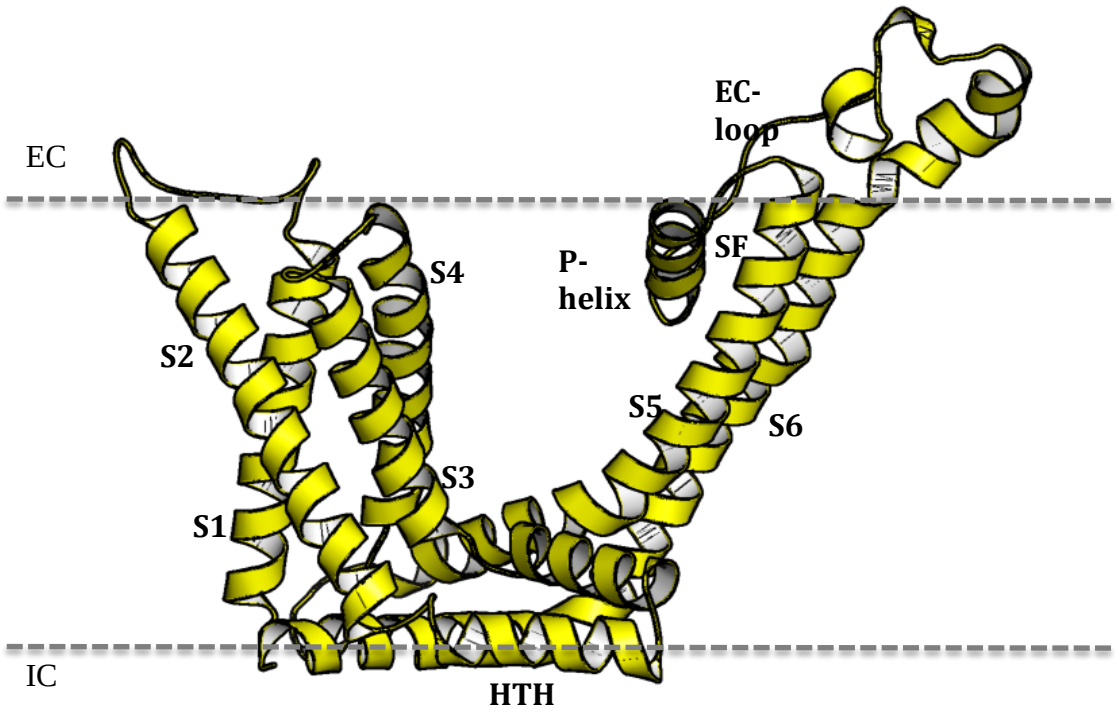


**Supplementary Figure S3.** A monomeric chain of TRPM8 TM region (yellow) as positioned in the lipid bilayer. The top and the lower boundary of the lipid bilayer have been illustrated as a grey line. Four identical chains come together to form a functional channel

**Supplementary Figure S4:**

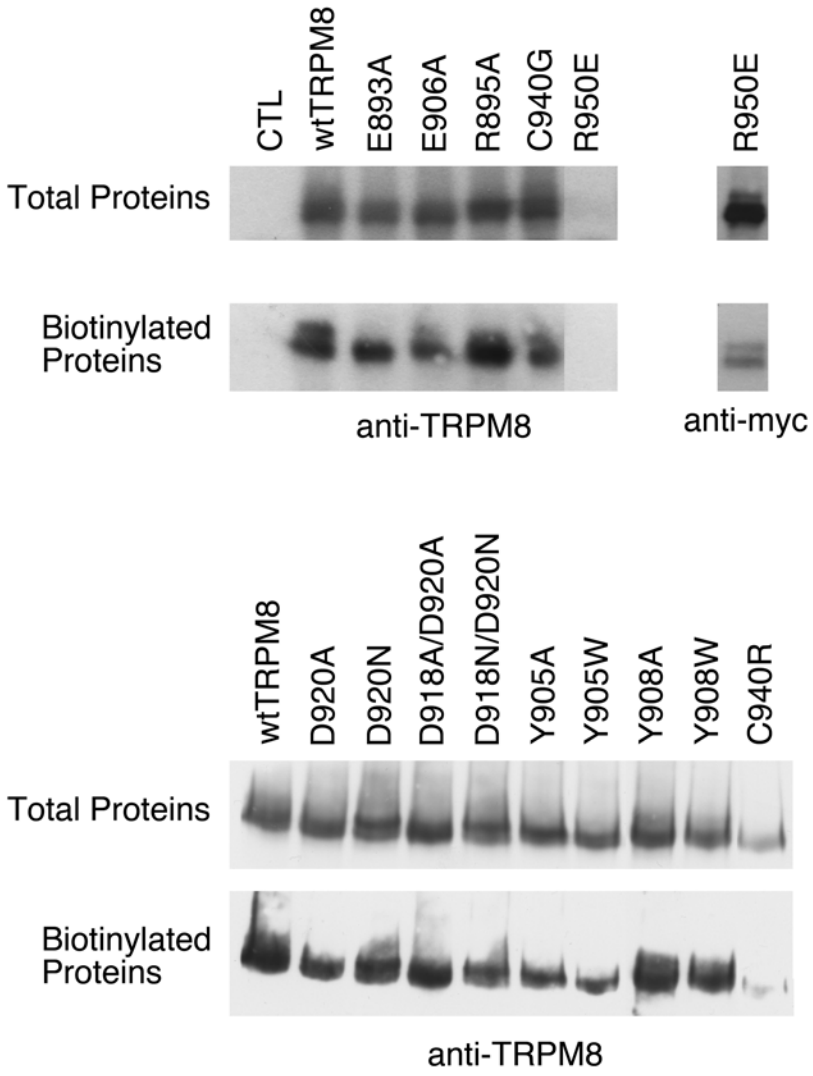


**Supplementary Figure S4**. Cell surface biotinylation of *wild-type* and mutant TRPM8 proteins in HEK cells. Immunoblottings showing the detection of TRPM8 proteins in total protein extracts (Total Proteins) after pull-down of biotinylated proteins with neutravidin beads (Biotinylated Protein). Proteins were detected with antiTRPM8 antibody except TRPM8 ($R^{950}A$), which was revealed with anti-myc antibody.

**Supplementary Figure S5:**

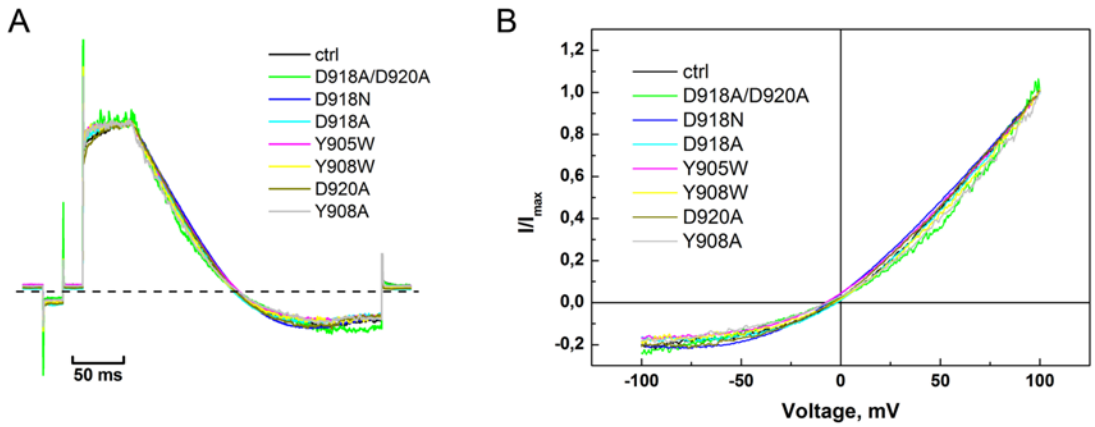


**Supplementary Figure S5.** TRPM8 mutant proteins exhibit unaltered electrophysiological properties. **A**: Normalized whole-cell traces of representative cells transfected with wild type (ctrl) or mutant TRPM8 proteins and stimulated with the voltage ramp protocol presented above. Corresponding current/voltage relationships are shown in **B**.

**Supplementary Figure S6:**

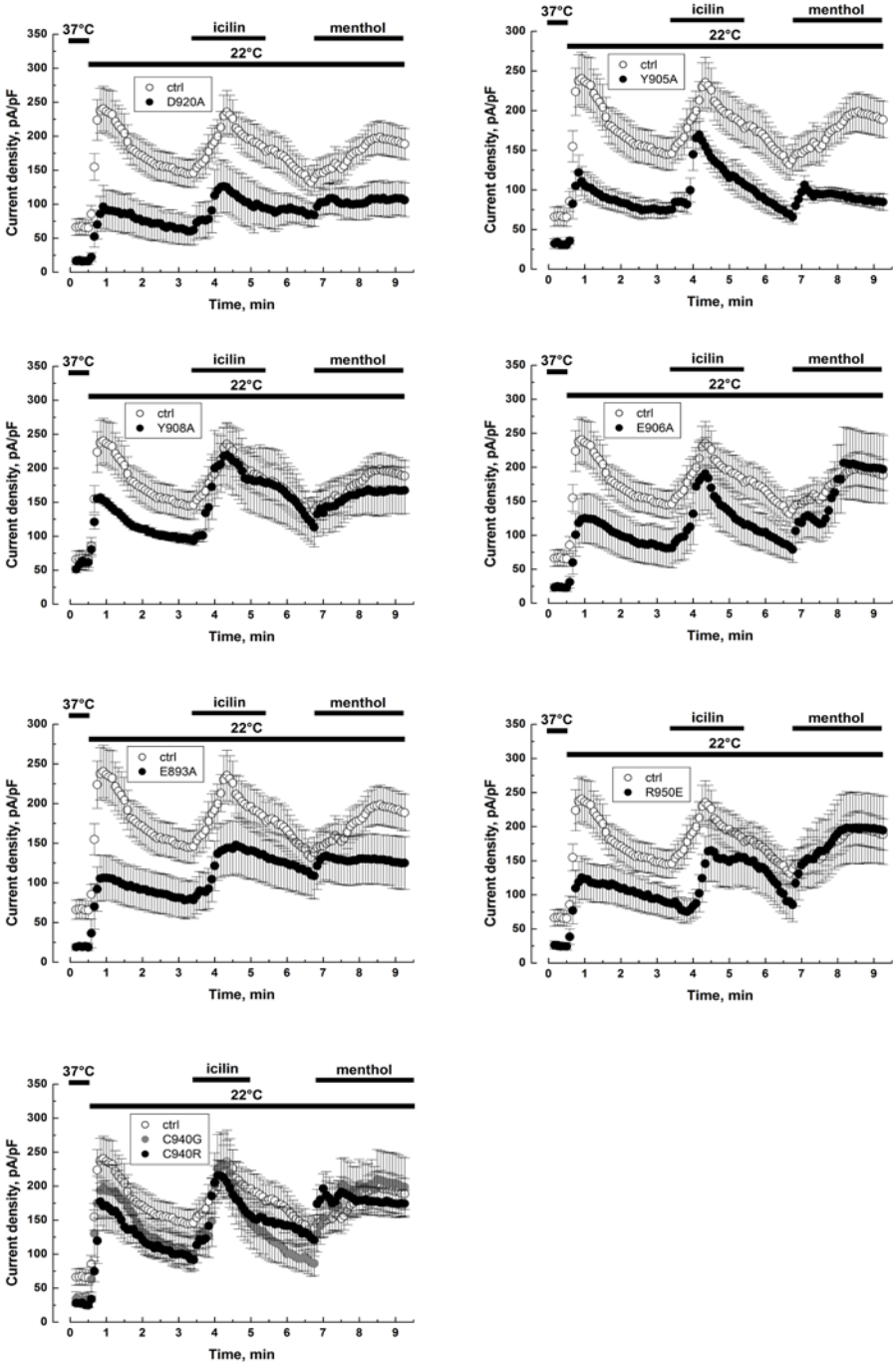


**Supplementary Figure S6**. Whole-cell recordings at +100mV of TRPM8 currents induced with either cold (22°C), or Icilin (10 µM), or Menthol (500 µM) for HEK cells concomitantly transfected with wild type TRPM8 and one specific TRPM8 mutant at a ratio 1:3. Cells transfected with wild type TRPM8, alone, were used as control (ctrl).

**Supplementary Table S1:**

| Plasmid | **Peak current (pA/pF), Cold (22°C)** | **Peak current (pA/pF), Icilin (10 µM)** | **Peak current (pA/pF), Menthol (500 µM)** |
|---|---|---|---|
| CTL | 187.1±40 | 183.2±75.8 | 168.5±56.2 |
| D918A | 162.4±54 | 165.4±52 | 173.9±51.7 |
| D918N | 159.1±37.6 | 154±33.6 | 145±32.8 |
| D918E | 139.7±43.2 | 190.3±49 | 110.6±19.9 |
| D920A | 128.8±34.5 | 119.1±40.2 | 130.7±23.5 |
| D920N | 13.7±6.3 | 9.4±2.1 | 8.8±1.4 |
| D918A/D920A | 28.2±10.4 | 31.6±9.3 | 21.4±4.7 |
| D918E/D920E | 223.8±30.5 | 164.8±13.9 | 170.7±23.1 |
| D918N/D920N | 6.3±1.1 | 31.6±9.3 | 21.4±4.7 |
| V919I | 222.1±69.2 | 228.6±53 | 166.5±33.9 |
| Y905A | 4.4±0.4 | 7.1±1.5 | 6.7±2.1 |
| Y905W | 57.9±16.7 | 64.4±23.2 | 84.1±23.2 |
| E893A | 7.5±2.3 | 23.4±9.8 | 26.4±11.1 |
| E906A | 38.2±23.6 | 24.6±17.4 | 17.4±11.2 |
| R950E | 5.9±0.6 | 6.2±0.8 | 11.5±3.5 |
| Y908A | 62.8±25.3 | 241.8±92.3 | 102.5±8.9 |
| Y908W | 87.7±25 | 157.2±48 | 109.2±31.6 |
| C940G | 4.3±0.6 | 3.9±1.5 | 3±0.1 |
| C940R | 13.4±9.2 | 3.5±0.3 | 3.3±0.5 |

**Supplementary Table S1.**

Summary of our patch-clamp results on single TRPM8 mutants when expressed in HEK293. Control (CTL) represents wild-type TRPM8 expressed in the same model. All data are presented as mean±SEM and show current density values obtained at +100mV following application of cold, icilin or menthol (n=3-8).